AIAA-2000-0094

Study of Mixing Enhancement Observed with a Co-annular Nozzle Configuration

K. B. M. Q. Zaman
NASA Glenn Research Center
Cleveland, OH 44135

and

D. Papamoschou
University of California at Irvine
Irvine, CA 92697

38th Aerospace Sciences Meeting & Exhibit
10-13 January 2000 / Reno, NV

Study of Mixing Enhancement Observed with a Co-annular Nozzle Configuration

K. B. M. Q. Zaman
Turbomachinery & Propulsion Systems Division
NASA Glenn Research Center
Cleveland, OH 44135

and

D. Papamoschou
Department of Mechanical & Aerospace Engineering
University of California at Irvine
Irvine, CA 92697

Abstract

Jet spreading enhancement with a certain coannular nozzle configuration has been explored. When the outer nozzle is flaired (i.e., made convergent-divergent) the ensuing jet spreads faster than the case where the outer nozzle is convergent. The spreading enhancement is most pronounced when the outer flow is run near 'transonic' condition, in an overexpanded state. Under this condition, the increased spreading takes place regardless of the operating conditions of the inner jet. This observation, first made in a small-scale facility (Ref. 1), has been confirmed and studied in some detail in a larger-scale facility. Results of the latter experiment are presented in this paper. The spreading increase is shown to be substantial and comparable to or better than that achieved by a lobed nozzle. Estimates based on idealized flow indicate that there is an accompanying thrust penalty – the actual penalty is expected to be less than the estimate but remains undetermined at this time. In both the earlier and the present experiments, the spreading increase has often been found to accompany a flow resonance. The nature of this resonance is addressed in this paper. It is shown that the spreading increase takes place even if the resonance is absent. Thus, flow excitation due to the resonance is ruled out as the underlying mechanism. While the complete mechanism remains unclear, it is conjectured that pressure gradients near the nozzle, characteristic of overexpanded flow, are at the root of the phenomenon.

1. Introduction

With a coannular nozzle configuration, when the outer annular flow is run at specific off-design conditions, as elaborated in the following, the ensuing jet flow is found to spread faster than that in 'normal' conditions. The phenomenon has been first observed by the second author in earlier experiments at UC Irvine and a patent filed by UC is pending on the nozzle configuration and conditions that would provide such mixing enhancement. Key features of the earlier UCI findings are covered in a companion paper (Ref. 1). The phenomenon is attractive because mixing enhancement is often desired in aircraft engine exhausts. (In this paper, the attributes of jet 'spreading' and 'mixing' are used interchangeably assuming one directly follows the other). Furthermore, many aircraft nozzle systems involve coannular configurations and it would appear that the observed phenomenon could be induced by relatively simple design changes. This led to an examination of the UCI observation by the first author who has been involved in research on methods for mixing enhancement in aircraft propulsion applications.

The UCI observation: Enhanced mixing was observed when the outer nozzle was 'flaired', i.e, made convergent-divergent, and the outer flow was run at 'transonic' conditions. Under those conditions, the centerline Mach number decay was found to be significantly faster than that observed in the case when the outer nozzle was simply convergent. Mixing enhancement was most pronounced when the outer flow 'Mach number' ranged between 0.8 and 1.2. The phenomenon was robust, repeatable and occurred for a wide range of operating conditions for the inner flow. It was also observed that a flow resonance accompanied the enhanced mixing process. It was thought that the flow instability instigated by the resonance broke up the jet into large vortices and that this might be the underlying mechanism for the enhanced mixing.

Objectives: The present investigation was undertaken, first, in order to independently confirm the phenomenon in a different facility. Second, a demonstration of its occurrence with larger-scale nozzles was desired. The UCI results were obtained with a small-scale facility (inner jet diameter was 1.27 cm) that could be subjected to questions regarding Reynolds number and initial condition effects. Approximately three times larger nozzle sizes were used in the present experiment in order to alleviate those concerns; the larger nozzles also permitted flow field surveys with adequate probe resolution. A third objective was to assess the thrust penalty. The final objective was to shed further light on the flow mechanisms of the mixing enhancement process.

2. Experimental Procedure

The experiment was conducted in an open jet facility at NASA Glenn Research Center. Existing dual-flow hardware was adapted for the study. The hardware consisted of a 14 cm diameter pipe section that attached to a jet facility to provide the inner (primary) flow. An annular plenum chamber surrounded the pipe section and provided the outer (secondary) flow. The flow to the outer chamber was supplied through four equally spaced ports and then routed through contoured interior and screens to provide a uniform annular stream at the exit. The inner and outer streams generated by the dual-flow hardware were then passed through contoured coannular nozzles. A schematic diagram of the nozzles, attached to the exit of the dual-flow hardware, is shown in Fig. 1(a). A perspective view of only the nozzles is shown in Fig. 1(b).

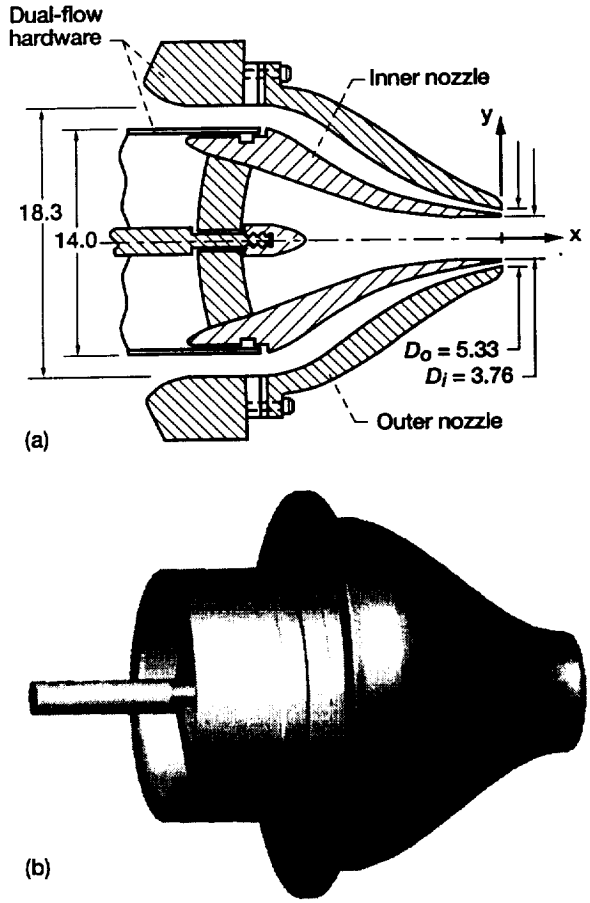

Figure 1.—Coannular nozzle configuration. (a) Schematic with dimensions in cm. (b) Perspective view; for 'Nozzle 1' the outer annular passage is convergent, for 'Nozzle 2' the outer passage is convergent-divergent with $M_D \approx 1.7$.

The dual-flow hardware had a 0.95 cm diameter 'sting', held by a set of three struts, for attaching center-bodies. In the present experiment, the sting was used to hold the inner nozzle via a second set of airfoil-shaped struts. The inner nozzle fitted to the interior of the pipe section, as shown in Fig. 1(a). The outer nozzle bolted to the end of the dual-flow hardware. Ring shaped plugs were used during assembly to ensure concentricity of the two nozzles.

For all experiments, the inner nozzle remained fixed. This was a convergent-divergent nozzle

with a design Mach number of 1.28. The exit and throat diameters were 3.76 cm and 3.65 cm, respectively, and the throat-to-exit length was 1.27 cm. The lip thickness at the exit was approximately 0.75 mm. Results obtained with two outer nozzles are presented in this paper. The first had an interior contour such that, together with the outer shape of the inner nozzle, the flow converged all the way to the exit. The exit diameter of this nozzle was 5.33 cm. The second outer nozzle provided a convergent-divergent passage ending with the same nominal exit diameter as the first one. The throat was 2.54 cm upstream from the exit. The area ratio was such that the design Mach number would be about 1.7 if one-dimensional idealized flow could be assumed. In the following, the coannular nozzle system with the convergent outer one will be referred to as 'Nozzle 1', and the system with the convergent-divergent outer one will be referred to as 'Nozzle 2'. As a reminder of the shapes, these will be alternatively referred to as the 'convergent' and 'flaired' cases, respectively. The exit diameter of the outer nozzle will be denoted as 'D_o' and that of the inner nozzle as 'D_i'.

The nozzle dimensions were approximately three times larger than those in the UCI experiment. Thus, the present experiment involved about an order of magnitude larger mass flow rates. Separate, continuous, compressed air supplies were available for the inner and outer streams with independent controls. Orifice meters located on the supply lines provided mass flow rate data for each stream. The jet discharged into the ambient air of the test chamber. The experiment involved 'cold' flows, i.e., the total temperature was approximately the same throughout the flow and in the ambient.

Most of the data were obtained by Pitot probe surveys. Limited static pressure surveys were conducted in separate runs. All data were obtained under automated computer control, after allowing sufficient warm-up time to ensure steady-state flow conditions. The inner plenum pressure was held by feedback control. The data acquisition routine continually monitored the plenum and the ambient pressures as well as the pressures for the two orifice meters. The acquisition routine rejected any data if the inner plenum pressure deviated more than 1% of the set value; the outer plenum pressure did not have feedback control and data rejection limit was set for 2% of the set value.

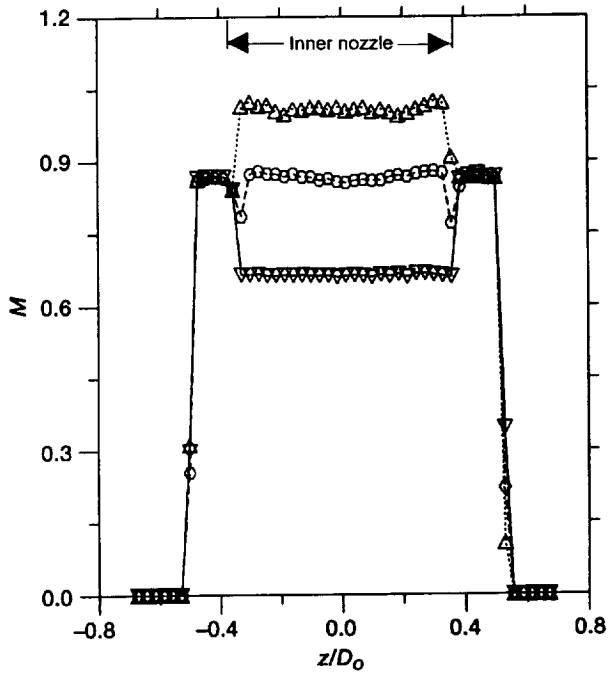

Figure 2.—Mach number profiles at the exit of Nozzle 1 (x/D_O = 0.05). Data are for inner jet Mach numbers (M_{ji}) of 1.02 (△), 0.86 (0) and 0.64 (▽); outer jet Mach number, $M_{jo} \approx 0.86$ for all cases.

3. Results and Discussion

Mach number profiles at the exit of Nozzle 1 (convergent case) are shown in Fig. 2. Here, the Mach number, M, is calculated simply from the total pressure (p_t) assuming static pressure to be equal to ambient pressure (p_a),

$$M=(((p_t / p_a)^{(\gamma-1)/\gamma}-1)\frac{2}{\gamma-1})^{1/2}$$

, γ being the ratio of specific heats. Notations M_{ji} and M_{jo} are used to denote 'jet Mach numbers' for the inner and outer streams based on the plenum pressures; i.e., these values are obtained by replacing p_t in the above expression with the respective plenum pressures. (Actual Mach number, based on total and static pressures measured at the same point, will be denoted as M_a.) In Fig. 2, data for three values of M_{ji} are shown while M_{jo} is held approximately a constant. The profiles show that the outer annular nozzle has yielded approximately uniform velocity distribution in spite of the complex flow path. The inner nozzle flow is also reasonably uniform except for some undula-

tions, presumably due to the two sets of struts in the flow path (§2). For the condition, $M_{ji} = M_{jo} \approx 0.86$, the wake from the inner nozzle lip can also be seen at this measurement station.

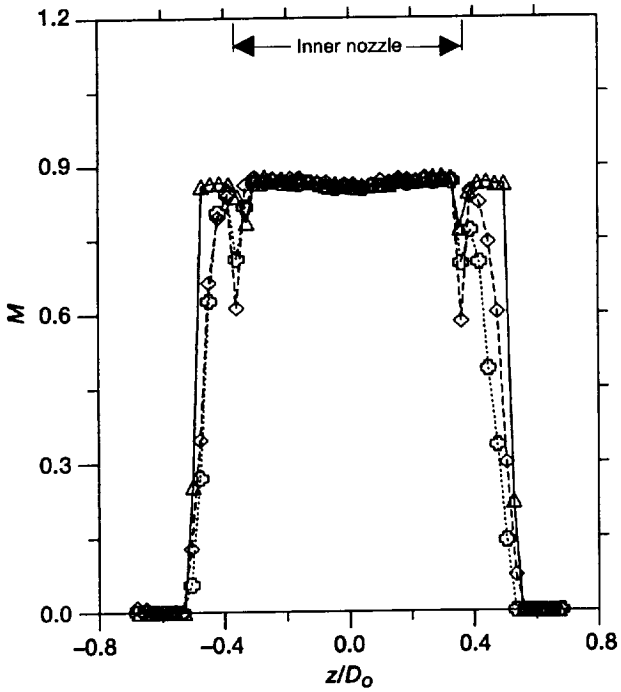

Figure 3.—Mach number profiles at the exit ($x/D_O \approx 0.05$): △, Nozzle 1; ◇, Nozzle 2; ⬡, Nozzle 2 (trip). $M_{ji} = M_{jo} \approx 0.86$ for all cases.

Corresponding Mach number profiles for, $M_{ji} = M_{jo} \approx 0.86$, obtained with Nozzle 2 (flaired case) are compared with data for Nozzle 1 in Fig. 3. Two sets of data are shown for the flaired case; one set is for a clean interior of the outer nozzle while the other is with boundary layer trip placed just upstream of the throat. The significance of the tripped boundary layer case will be discussed later in the text. First, the difference between Nozzle 2 (clean case, diamond symbols) and Nozzle 1 case (triangular symbols) is examined. It can be seen that the velocity profiles for the outer annulus are 'narrower' with Nozzle 2. Even though the exit area is the same, the throat for the outer annulus with Nozzle 2 has a smaller area and this causes a smaller flow rate at the given plenum pressure. Flow separation in the diverging section is also likely. These factors apparently result in the observed profile for Nozzle 2.

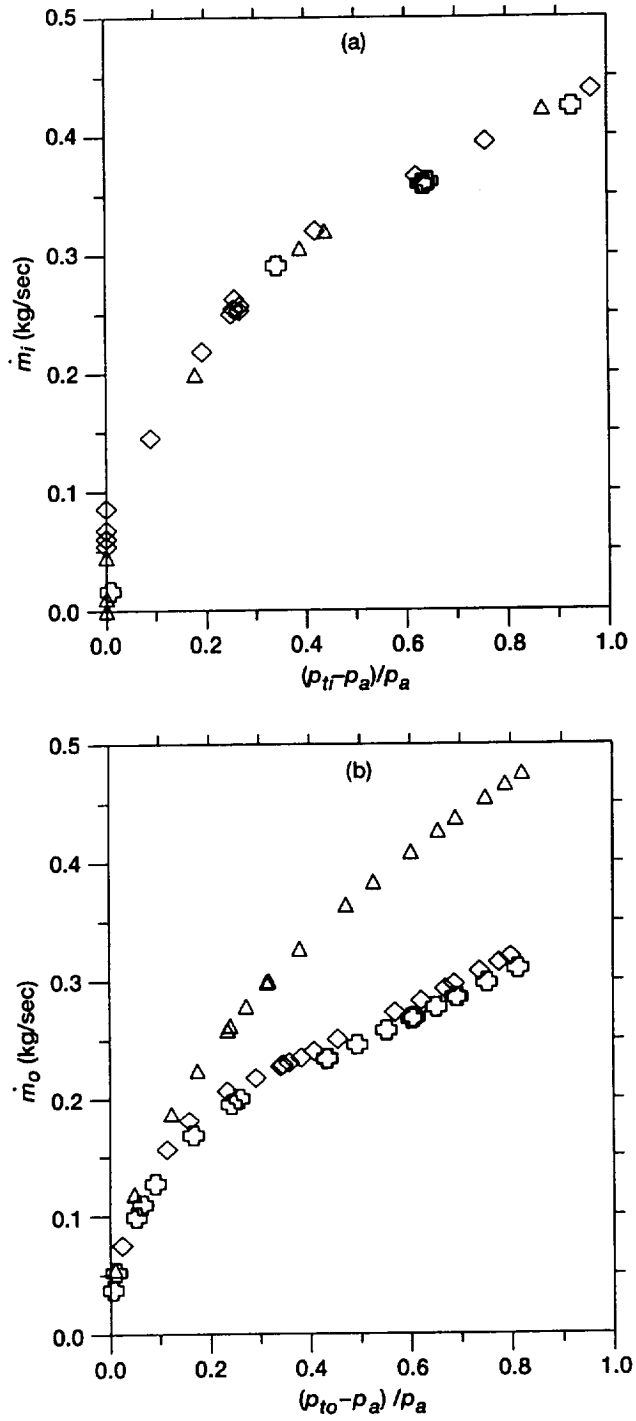

Figure 4.—Mass flow rate versus plenum pressure: △, Nozzle 1; ◇, Nozzle 2; ⬡, Nozzle 2 (trip). (a) Inner (primary) flow; for the two clusters of data at $(p_{ti}-p_a)/p_a = 0.25$ and 0.63, outer plenum pressure $(p_{to}-p_a)/p_a$ was varied from 0 to 0.9. (b) Outer (secondary) flow; $(p_{ti}-p_a)/p_a \approx 0.64$ for all cases.

Mass flow rates ($\dot{m}$) for the inner and outer nozzles, measured by orifice meters, are shown in Figs. 4(a) and (b) as a function of the respective plenum pressures. Here, p_{ti} and p_{to} represent total pressures in the inner and the outer plenum chambers, respectively. The data in Fig. 4(a) show that the inner nozzle flow rate remains unaffected when the outer nozzle is changed. The flow rate depends on the plenum pressure (p_{ti}) and practically remains unaffected by the outer plenum pressure (p_{to}); two sets of data in the figure, identified in the caption, demonstrate this. The relatively lower mass flow rate ($\dot{m}_o$) for the outer annulus with Nozzle 2, compared to Nozzle 1 case, is clearly evident in Fig. 4(b). The flow rate for Nozzle 1 (convergent case, triangular symbols) is larger than that of Nozzle 2 (flaired case), from about $(p_{to}-p_a)/p_a$ = 0.25 up to the maximum pressure covered in the experiment. In this range of p_{to} the flow in the outer annulus of Nozzle 2 is expected to have shocks, as discussed later. This is also the range where enhanced mixing is expected based on the UCI observation. (For Nozzle 2, boundary layer trip makes little difference in the $\dot{m}$ data. As stated before, the tripped case data will be discussed shortly).

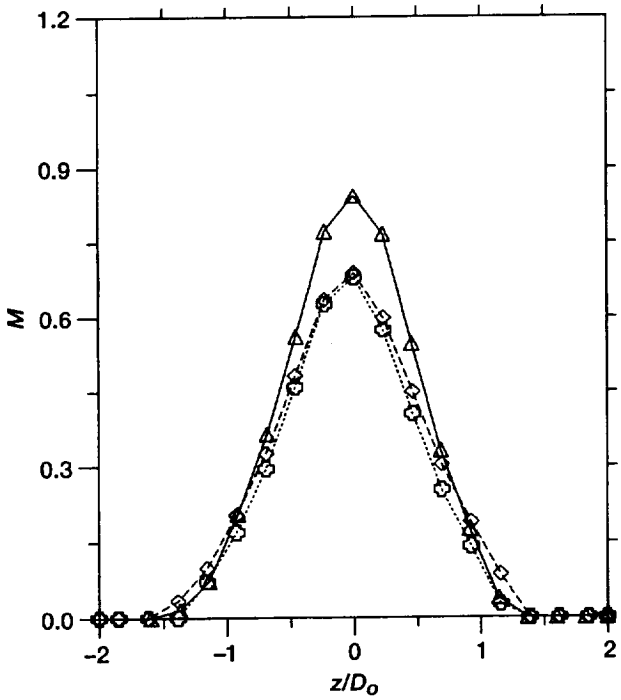

Figure 5.—Mach number profiles at x/D_o = 6 for the three cases of Fig. 3.

Cross-sectional profiles of Mach number (M) for Nozzles 1 and 2 are compared in Fig. 5, for x/D_o = 6, corresponding to the conditions of Fig. 3 ($M_{ji} = M_{jo} \approx 0.86$). A relative drop in the Mach number in the core of the jet with Nozzle 2 is evident. This implies a faster jet spreading with Nozzle 2 and is qualitatively in agreement with the UCI observation. However, as discussed in the foregoing, the outer mass flow rate $\dot{m}_o$ is less with Nozzle 2 and this must be taken into consideration for proper comparison of the jet spreading.

In order to account for the difference in the mass flow rates, an equivalent diameter D_{eq} is calculated based on the m data. For a given plenum pressure (assuming $p_{ti} = p_{to}$), D_{eq} is calculated to approximately represent the diameter of a convergent nozzle that would yield the same mass flow rate ($\dot{m}_i + \dot{m}_o$). Thus, corresponding to the condition $M_{ji} = M_{jo} \approx 0.86$ (Figs. 3, 5), D_{eq} for nozzle 2 is found to be smaller than that of Nozzle 1 by a factor of about 1.1, based on the data of Fig. 4. Values of D_{eq} obtained for this condition are assumed to be applicable at the other two operating conditions of Fig. 2.

Centerline Mach number distributions are now compared for Nozzle 1 and Nozzle 2 in Figs. 6(a)-(c), for the three operating conditions of Fig. 2. Streamwise distance x is normalized by D_{eq}, and the ordinate represents actual Mach number calculated from total and static pressures measured in separate runs. Evidence of a shock near the nozzle exit may be noted for all three sets of data, but this is more pronounced at higher M_{ji}. In all cases, the centerline Mach number decay with Nozzle 2 is found to be clearly faster than that with Nozzle 1. Thus, these data demonstrate that the jet spreading is indeed faster with the flaired outer nozzle, and this is true even when the discrepancy in the initial mass flow rates is accounted for. (It should be noted that had the distance x been nondimensionalized by the outer diameter D_o, the difference between the curves for Nozzles 1 and 2 would have been greater.)

As with the UCI observation, a flow resonance (see §1) also occurred with Nozzle 2 in the present experiment. The resonance was accompanied by a 'screech-like' tone. This tone was quite similar in characteristics to tones occurring with single convergent-divergent nozzles, studied previously (Ref. 2).

The salient features of the results of Ref. 2 are worth summarizing here. The tone was studied for a variety of single C-D nozzles. It occurred in 'transonic' conditions when a normal shock was expected within the

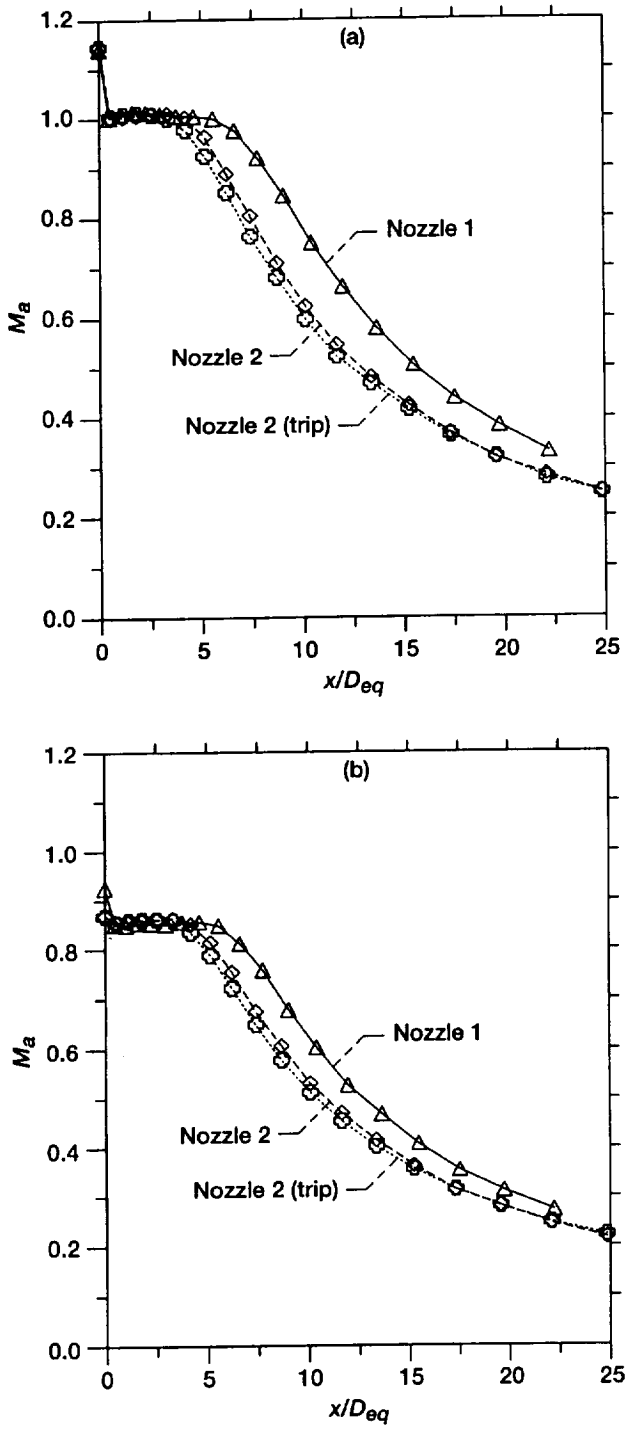

Figure 6.—(a) and (b).

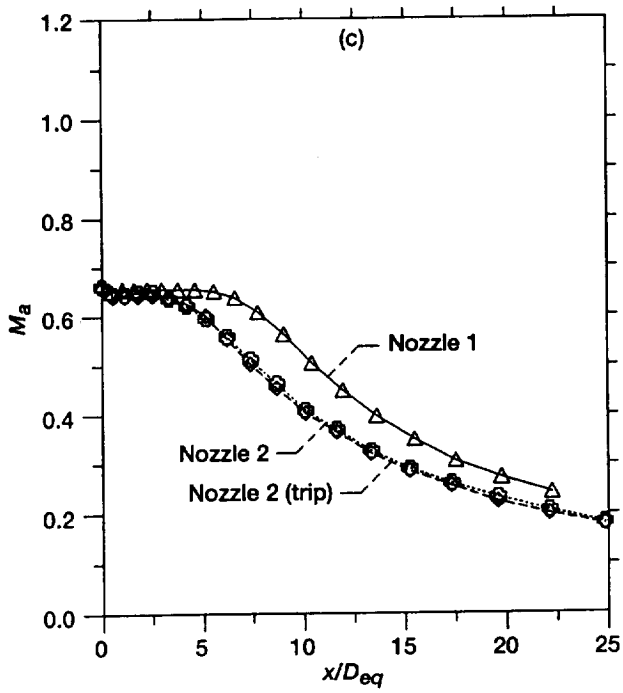

Figure 6.—Centerline variation of actual Mach number. (a) $M_{ji} = 1.02$, $M_{jo} = 0.86$. (b) $M_{ji} = 0.86$, $M_{jo} = 0.86$. (c) $M_{ji} = 0.64$, $M_{jo} = 0.86$.

diverging section or when the flow was in the early stages of overexpansion. While this tone could be easily confused with conventional screech noise (reader not familiar with the latter phenomenon is referred to the cited paper), it was shown to be different in characteristics and origin. For example, the frequency would increase with increasing plenum pressure, a trend opposite to that of screech noise. A 'tab' placed at the nozzle exit would completely eliminate screech while the tone under consideration would remain unaffected. Furthermore, the occurrence of the tone could be related to an unsteady boundary layer separation near the throat. This was evident from the fact that a boundary layer trip placed near the throat, (that would have no effect on screech), would weaken or completely suppress the tone.

The flow resonance and the accompanying tone with the flaired coannular nozzle behaved in a similar manner as described above. This is shown by the sound pressure data in Figs. 7-9, measured by a microphone located approximately 90° to the jet axis and $30D_O$ away from the nozzle.

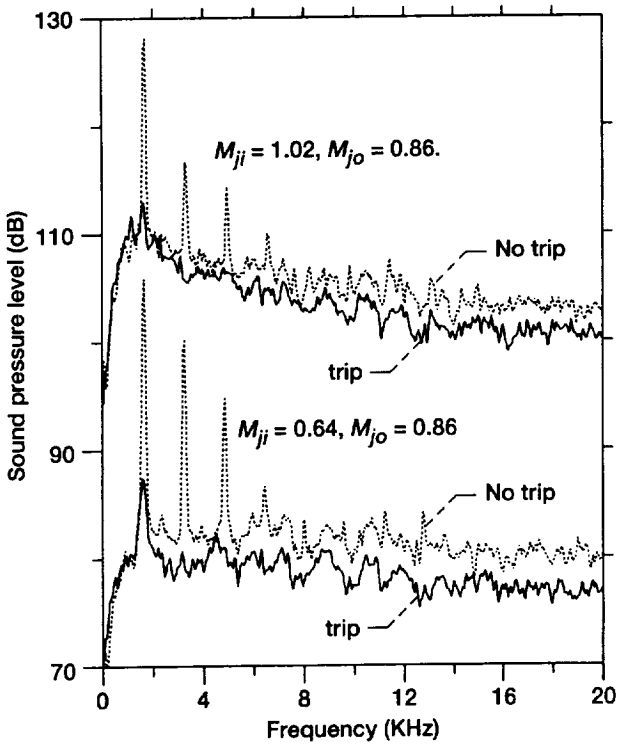

Figure 7.—Sound pressure spectra for Nozzle 2 with and without boundary layer trip near the throat, for indicated operating Mach numbers; upper pair shifted by 20 dB.

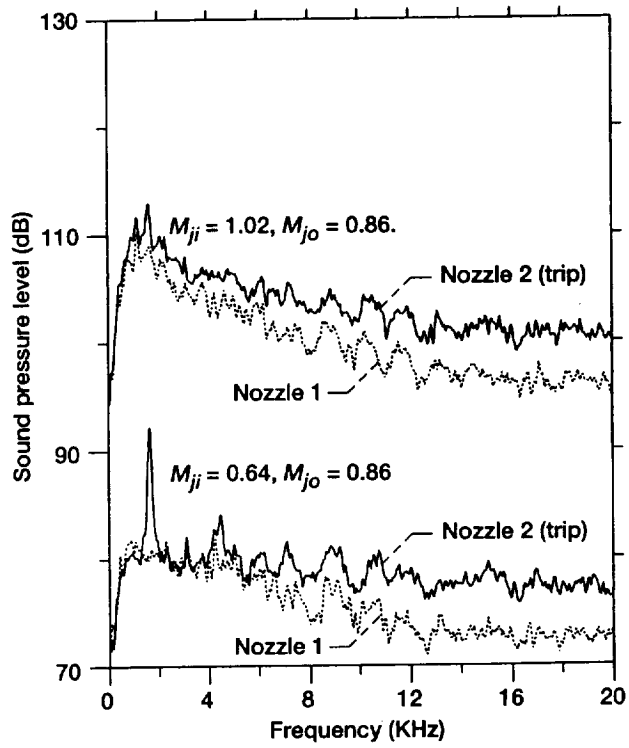

Figure 8.—Sound pressure spectra for Nozzle 2 (with boundary layer trip) and Nozzle 1, for indicated operating conditions; upper pair shifted by 20 dB.

In Fig. 7, sound pressure spectra are compared with and without a boundary layer trip for Nozzle 2 corresponding to two operationg conditions of Fig. 2. A tone at 1625 Hz dominates the spectra for the untripped case. The boundary layer trip practically eliminates the tone. (The trip consisted of four beads of epoxy placed on the inner surface of the outer nozzle just prior to the throat.) As with the single nozzles (Ref. 2), the tone was characteristic of the convergent-divergent geometry and did not occur with the convergent nozzle. This is evident from the corresponding noise spectra for Nozzle 1, compared to the data for Nozzle 2 (tripped), in Fig. 8. Note that the data for Nozzle 2 in the latter figure represent another run with reapplication of the epoxy beads. The tone was sensitive to small variations in the geometry of the boundary layer trip, and this explains some difference in the data for Nozzle 2 between Figs. 7 and 8.

The tone frequency variation with the outer plenum pressure for Nozzle 2 is shown in Fig. 9. The frequency increases with increasing plenum pressure (and hence with M_{jo}). This is a trend similar to that observed with single C-D nozzles, as mentioned before. The solid and open data symbols, for operating conditions explained in the caption, also demonstrate that the tone is practically independent of the inner flow setting. (It should be mentioned here that with the outer flow off, the inner nozzle also underwent a resonance at transonic conditions commensurate with the results of Ref. 2. However, when the outer flow was turned on, its tone dominated the noise field and the tone from the inner flow was obliterated in the spectrum.) In figure 9, flow regimes *I*, *II*, *III* and *IV* are marked; these are based on one-dimensional analysis and represent fully subsonic state, a state with a normal shock in the diverging section, and overexpanded and underexpanded states, respectively. These flow regimes are determined simply from the throat-to-exit area ratio of the outer flow. The tone can be seen to occur in regimes *II* and *III*. This was also the case with single nozzles as reported in Ref. 2. Thus, the tone observed with the 'flaired' coannular nozzle, in the present as well as the UCI experiment, is inferred to be of the same origin as that reported in Ref. 2.

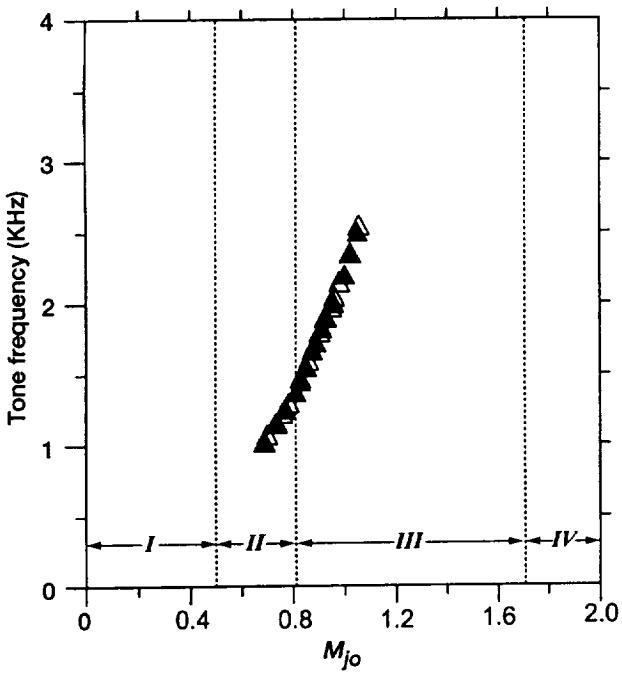

Figure 9.—For Nozzle 2, tone frequency versus outer jet Mach number. Open data points for M_{ji} = 0; solid data points for $M_{ji} \approx 0.30$.

The significance of the data for the tripped boundary layer case with Nozzle 2, presented in Figs. 3 – 6, should now be clear. The effect of the flaired outer nozzle, on the observed increase in jet spreading, remains practically the same whether or not there is a boundary layer trip. This can be seen from the lateral Mach number profiles in Fig. 5 as well as the centerline profiles in Fig. 6. Since the boundary layer trip suppresses the flow resonance and the tone, flow excitation due to the tone, therefore, is ruled out as the primary mechanism for the observed spreading increase.

Unfortunately, the full mechanism has remained unclear at this time. One may speculate that pressure gradients near the nozzle exit owing to the overexpanded state might be playing a role. With an overexpanded flow, the static pressure at the nozzle exit is subambient. Thus, the jet in the vicinity of the nozzle exit is subjected to streamwise as well as lateral pressure gradients. This may not only affect momentum transfer in the lateral direction but also the stability characteristics of the jet. (Exit static pressure based on idealized flow calculation is discussed with estimates of thrust in the following. Static pressure in the outer stream could not be measured with confidence during these experiments due to flow unsteadiness and facility constraints.) Further investigation is currently under way with single C-D nozzles in an attempt to address the flow mechanisms. In the following, the spreading increase observed with Nozzle 2 is assessed further. The increase is compared with that achieved by other techniques and an attempt is made to evaluate the thrust penalty.

The $M_{ji} = M_{jo} \approx 0.86$ case is similar to a single nozzle operation, having approximately uniform velocity distribution at the exit. Jet spreading and thrust for this condition are thus amenable for ready comparison with single nozzle data. Mach number distributions on the cross sectional plane for this condition are shown in Fig. 10, for $x/D_{eq} \approx 14$. An increased spreading with Nozzle 2 (with or without trip), relative to Nozzle 1, is not apparent at first glance. However, an inspection reveals that the area covered by a given contour for either case of Nozzle 2 is somewhat larger than that for Nozzle 1. The peak Mach number in the measurement domain is also significantly lower with Nozzle 2. Overall characteristics of these flow fields are compared in the table below.

Nozzle	M_{ji}	M_{jo}	$\dot{m}_i$ (kg/s)	$\dot{m}_o$ (kg/s)	D_h / D_o y-axis	D_h / D_o z-axis	Peak M	$\dot{m} / (\dot{m}_i + \dot{m}_o)$
1	.861	.862	.359	.422	2.19	2.26	.45	3.61
2	.861	.864	.368	.286	2.56	2.50	.36	4.20
2 (trip)	.860	.865	.368	.272	2.43	2.60	.35	4.16

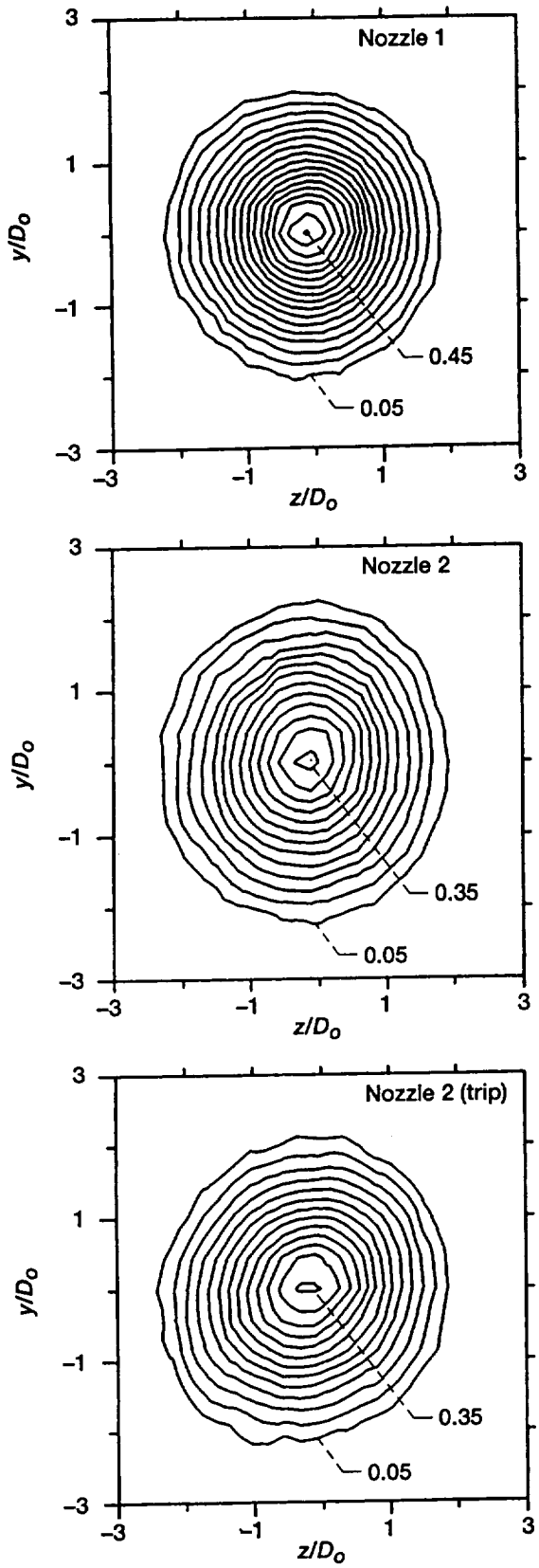

Figure 10.—M contours at $x/D_{eq} \approx 14$; $M_{ji} = M_{jo} \approx 0.86$ for all cases.

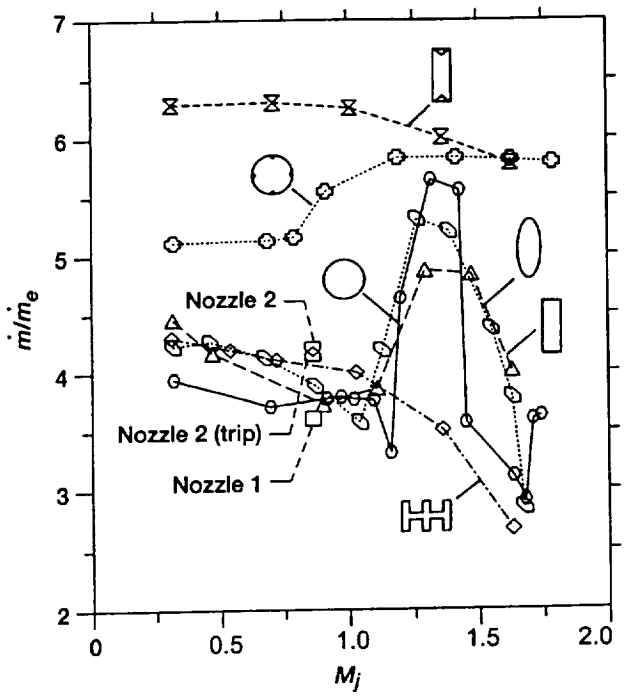

Figure 11.—Axial mass flow rate, measured at $x/D_{eq} \approx 14$, compared to data for single nozzle cases (ref. 3). The three data points for the present cases correspond to $M_j = M_{ji} = M_{jo} \approx 0.86$.

Here, D_h represents 'half velocity diameter' of the jet's cross-section. Data in the last column represent longitudinal mass flow rate, obtained from appropriate integration of the total pressure data, and normalized by the measured initial mass flow rates. For further details of data reduction the reader may look up Ref. 3. It should be clear from these data that there is a small but definite increase in jet spreading with either version of Nozzle 2 when compared to the Nozzle 1 case.

The mass flux data for the present coannular jets are now compared in Fig. 11 with corresponding data for a variety of single nozzle cases. The nozzle exit geometry for each case is indicated schematically with each curve. There are data from a rectangular, an elliptic, a 6-lobed, a circular and two cases of tabbed nozzles (Ref. 3). All data are for $x/D_{eq} = 14$, and shown as a function of the jet Mach number. The three data points from the current experiment are identified in the figure. There are many factors that affect jet spreading and for a full discussion of the trends in this figure the reader is referred to the cited reference. Here, we simply note that with the UCI design, at $M_j = 0.86$, a substantial increase in the fluxes has been

achieved for Nozzle 2, both tripped and untripped. An approximately 15% increase in the flux has occurred with the flaired configuration when compared to the convergent configuration. The increase can be seen to be better than that achieved by the 6-lobed nozzle. It should also be clear that other factors, such as screech at higher M_j and tabs, can result in a much higher increase in the spreading. It is needless to say, however, that the comparison in Fig. 11 is limited in scope. Only data with the same inner and outer jet Mach number for the coannular case could be compared. The UCI design is consistently effective for a wide range of inner-to-outer jet Mach number ratios that cannot be readily compared with single nozzle data.

Since the enhanced spreading with the flaired nozzle is achieved when it is run in an overexpanded state, there should be an accompanying thrust penalty. This is considered now. Thrust for the coannular case is estimated by assuming the inner and outer flows to be independent of each other. Ideal, one-dimensional nozzle flow assumptions (e.g., Ref. 4) are made for each stream. Furthermore, calculations are made for the condition $M_j = M_{ji} = M_{jo}$. For a given plenum pressure (i.e., a given M_j), the ideal thrust for the two flows is calculated independently from the equation,

$$T_{ideal} = A_e \rho_e U_e^2 + (p_e - p_a) A_e ,$$

where A represents the nozzle cross-sectional area and the sbscript 'e' represents conditions at the nozzle exit. The throat-to-exit area ratio of each stream is used to determine the properties at the exit (Refs. 2,3). For a given stream with given plenum pressure p_t, the maximum available thrust is also calculated using the following expression (Ref. 4),

$$T_{\max} = p_t A_e \left[\frac{2}{\gamma - 1} \left(\frac{2}{\gamma + 1} \right)^{\frac{\gamma+1}{\gamma-1}} \left(1 - \left(\frac{p_a}{p_t} \right)^{\frac{\gamma-1}{\gamma}} \right) \right]^{1/2}$$

Note that whereas T_{ideal} represents the ideal thrust for the given nozzle geometry, T_{max} represents the maximum available thrust that would be obtained if the flow were expanded fully using an appropriate C-D nozzle. These thrusts for both inner and outer streams are thus calculated for each M_j. The ratio of the summations of the two ideal thrusts and the two maximum thrusts is the thrust coefficient, C_f.

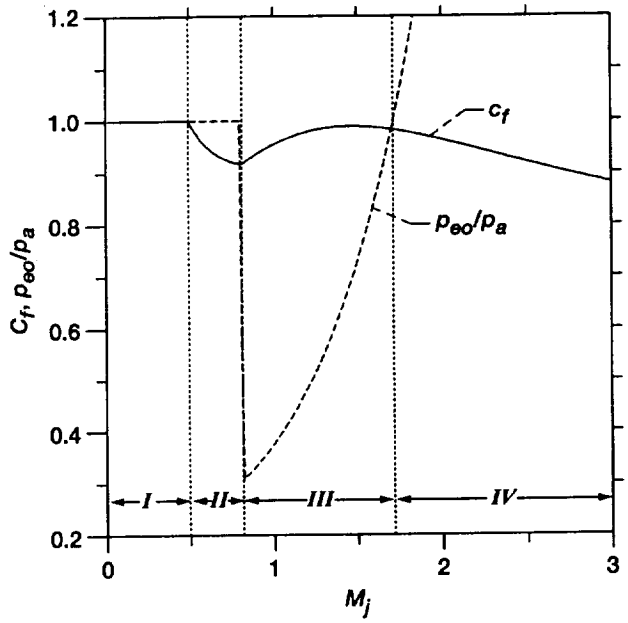

Figure 12.—Estimated thrust coefficient (C_f) versus jet Mach number (M_j) for nozzle 2; $M_j = M_{ji} = M_{jo}$. Static pressure p_{eo} is for exit of outer flow based on ideal, one-dimensional calculation.

The variation of C_f with M_j for Nozzle 2 is shown in Fig. 12. Also shown in this figure is the variation of the calculated static pressure at the exit of the outer stream. As with Fig. 9, the flow regimes *I* – *IV* pertain to the nozzle. In the subsonic regime (*I*), C_f is calculated to be unity (assumes no flow separation or losses due to skin friction). In regime *II*, a normal shock is expected within the diverging section. In this flow regime, C_f decreases with increasing M_j. With further increase in M_j, at the onset of the overexpanded regime (*III*), the normal shock is at the nozzle exit when C_f reaches a minimum. At this condition, the static pressure at the nozzle exit goes through a discontinuity due to the passage of the shock. With further increase in M_j in regime *III*, C_f increases as the outer flow approaches the fully expanded condition. At the latter condition (boundary between regimes *III* and *IV*), $p_{eo} = p_a$; however, C_f is less than unity since the inner flow is underexpanded. The maximum in C_f occurs at $M_j \approx 1.45$ for the given geometry. Note that the maximum is still less than unity since neither

stream is perfectly expanded. With even further increase in M_j in regime *IV*, C_f continues to decrease as both streams become increasingly more underexpanded.

Thus, it is apparent that in the flow regime where the increased jet spreading is achieved, there is a significant thrust penalty. For example, at $M_j = M_{jo} = M_{ji} = 0.86$, C_f is about 0.93. Thus, the 15% increase in the mass flow rate (at $x/D_{eq} \approx 14$; Fig. 11) has been achieved at the expense of an estimated 7% thrust loss. However, it should be borne in mind that the thrust estimate is based on idealized flow calculations. In fact, thrust loss in pactice at the operating conditions under consideration may be less than the prediction. Such an expectation is based on past studies of overexpanded flows from single C-D nozzles. The idealized inviscid flow calculation assumes no flow separation and ignores boundary layer effects. In practice the flow often separates within the diverging section of the nozzle. With reference to the flow regimes in figures 9 and 12, such viscous effects may be particularly pronounced in regimes *II* and *III*. The onset of regime *III* may be delayed to higher M_j. The effect of these deviations from idealized assumptions, interestingly, can lead to thrust performance better than the prediction. "Separation moves the detachment point upstream, causing a change in the effective nozzle geometry to one that is shorter and has a lower expansion ratio. For a given NPR, this alleviates overexpansion and improves thrust efficiency" (Ref. 5). Thus, the 7% thrust loss with the present nozzle is likely to be an overestimate. The issue of actual thrust loss vis-à-vis mixing enhancement due to overexpansion is also being investigated with single C-D nozzles and will be reported in a future publication (some preliminary results were included in a recent review paper; Ref. 6).

4. Conclusions

An increase in the spreading of a coannular jet achieved through the use of a flaired outer nozzle has been studied in some detail. The spreading increase is found to be significant. For example, it is comparable or better than that achieved by non-axisymmetric (i.e., rectangular or elliptic) or lobed nozzles. Estimates based on idealized flow indicate that there is an accompanying thrust penalty. However, the penalty in practice is expected to be less than the idealized prediction. The actual extent of the penalty has remained undetermined at this time. The spreading increase is often found to accompany a flow resonance. The nature of this resonance is addressed in this paper. It is shown that the resonance is similar in origin to phenomenon studied previously for single C-D nozzles. It is accompanied by a screech-like acoustic emission and it occurs due to an unsteady boundary layer separation near the throat. It can be suppressed by appropriate boundary layer tripping. These characteristics of the resonance are verified for the present co-annular nozzle configuration. Significantly, it is shown that the spreading increase takes place even if the resonance is suppressed. Thus, flow excitation due to the resonance is ruled out as the underlying mechanism. While the complete mechanism remains unclear, it is conjectured that adverse pressure gradients near the nozzle, characteristic of overexpanded flows, are at the root of the observed phenomenon.

Acknowledgement

This work has been supported by Aerospace Propulsion and Power Research and Technology Base Program at NASA Glenn.

References

1. Papamoschou, D., "Mixing enhancement using axial flow", *AIAA paper 00-0093*, 38th AIAA Aerospace Sciences meeting, Reno, NV, 2000.

2. Zaman, K.B.M.Q. and Dahl, M.D., "Aeroacoustic resonance with convergent-divergent nozzles", *AIAA paper 99-0164*, 37th AIAA Aerospace Sciences meeting, Reno, NV, 1999.

3. Zaman K.B.M.Q., "Spreading characteristics of compressible jets from nozzles of various geometries", *J. Fluid Mech.*, 383, pp. 197-228, 1999.

4. Shapiro, A.H., "The dynamics and thermodynamics of compressible fluid flow", The Ronald Press Co., New York, 1953.

5. Hunter, C.A., "Experimental, theoretical, and computational investigation of separated nozzle flows", *AIAA Paper 98-3107*, 34th Joint Propulsion Conference, July, 1998.

6. Zaman K.B.M.Q., "Jet spreading increase by passive control and associated performance penalty", *AIAA paper 99-3505*, 30th AIAA Fluid Dynamics Conference, Norfolk, 1999.